Circulation: Arrhythmia and Electrophysiology

ORIGINAL ARTICLE

Action Potential Morphology Accurately Predicts Proarrhythmic Risk for Drugs With Potential to Prolong Cardiac Repolarization

William Lee, BSc, MBBS(Hons), PhD, DRCPSC*; Ben Ng, BSc(Med), PhD*; Melissa M. Mangala, BSc(Hons), PhD; Matthew D. Perry, BSc(Hons), PhD; Rajesh N. Subbiah, MBBS, PhD; Jamie I. Vandenberg, BSc(Med), MBBS, PhD; Adam P. Hill, BSc(Hons), PhD

BACKGROUND: Drug-induced or acquired long QT syndrome occurs as a result of the unintended disruption of cardiac repolarization due to drugs that block cardiac ion channels. These side effects have been responsible for the withdrawal of a range of drugs from market and are a common reason for termination of the development of new drugs in the preclinical stage. Existing approaches to risk prediction are expensive and overly sensitive meaning that recently there have been renewed efforts, largely driven by the comprehensive proarrhythmic assay initiative, to develop more accurate methods for allocation of proarrhythmic risk.

METHODS: In this study, we aimed to quantify changes in the morphology of the repolarization phase of the cardiac action potential as an indicator of proarrhythmia, supposing that these shape changes might precede the emergence of ectopic depolarizations that trigger arrhythmia. To do this, we describe a new method of quantifying action potential morphology by measuring the radius of curvature of the repolarization phase both in simulated action potentials, as well as in action potentials measured from induced pluripotent stem cell-derived cardiomyocytes. Features derived from the curvature signal were used as inputs for logistic regressions to predict proarrhythmic risk.

RESULTS: Optimal risk classifiers based on morphology were able to correctly classify risk to drugs in the comprehensive proarrhythmic assay initiative panels with very high accuracy (0.9375) and outperformed conventional metrics based on action potential duration at 90% repolarization, triangulation, and charge movement (qNet).

CONCLUSIONS: Analysis of action potential morphology in response to proarrhythmic drugs improves prediction of torsadogenic risk. Furthermore, morphology metrics can be measured directly from the action potential, potentially eliminating the burden of undertaking complex screens of potency and drug-binding kinetics against multiple cardiac ion channels. As such, this method has the potential to improve and streamline regulatory assessment of proarrhythmia in preclinical drug development.

GRAPHIC ABSTRACT: A graphic abstract is available for this article.

Key Words: arrhythmia ■ biomarkers ■ cardiac ■ morphology ■ Torsades de Pointes

Drug-induced or acquired long QT syndrome (aLQTS) is a potentially lethal condition associated with delayed repolarization of the cardiac myocyte, QT prolongation on the surface ECG and syncope or sudden cardiac death due to the arrhythmia Torsade de Pointes.[1] This proarrhythmic side effect of cardiac ion channel inhibition has resulted in the withdrawal of a range of drugs from the market over the past 30 years.[2] In practice, most drugs that cause acquired long QT syndrome do so primarily through block of the Kv11.1 potassium

Correspondence to: Adam P. Hill, BSc(Hons), PhD, Victor Chang Cardiac Research Institute, 405, Liverpool St, Darlinghurst, NSW 2010, Australia. Email a.hill@victorchang.edu.au
*W. Lee and B. Ng contributed equally as first authors.
Supplemental Material is available at https://www.ahajournals.org/doi/suppl/10.1161/CIRCEP.122.011574.
For Sources of Funding and Disclosures, see page 409.

Circulation: Arrhythmia and Electrophysiology is available at www.ahajournals.org/journal/circep

WHAT IS KNOWN?

- Regulatory guidelines around screening for proarrhythmic risk in preclinical drug development conventionally focus on activity against the hERG potassium channel and prolongation of repolarization.
- These metrics are now thought to be poor surrogates for risk that result in overly sensitive assays.
- Recent efforts have focused on identifying new metrics, more mechanistically linked to proarrhythmia, to allow more accurate risk classification.

WHAT THE STUDY ADDS

- The application of curvature analysis as a novel approach to measuring shape changes in the repolarization phase of the cardiac action potential that occur as precursors to early after depolarizations and arrhythmia.
- Metrics derived from curvature can categorize proarrhythmic risk of drugs with very high accuracy.
- The method can be applied to both in silico data, and to action potentials acquired from cardiomyocytes in vitro, so represents a flexible analysis that has significant potential as a new approach to the assessment of proarrhythmic risk in preclinical drug development.

Nonstandard Abbreviations and Acronyms

aLQTS	acquired long QT syndrome
APD_{90}	action potential duration at 90% repolarization
CiPA	comprehensive in vitro proarrhythmia assay
EAD	early after depolarization
Herg	human ether-a-go-go related gene
iPSC	induced pluripotent stem cell

channel (also known as human ether-a-go-go-related gene [hERG]).[3] Consequently, guidelines for preclinical safety screening of new drugs, described in the ICH S7B documents, have focused on drug potency against Kv11.1 and action potential prolongation as surrogates for Torsade de Pointes risk.[4,5] However, it is now accepted that while a hERG-centric screening is highly sensitive, it is not sufficiently specific, resulting in potentially inappropriate allocation of Torsade de Pointes risk and attrition of potential useful new therapeutic agents during early development.[6,7]

One aspect of cardiomyocyte electrophysiology that is now appreciated to be important in developing a more nuanced understanding of proarrhythmic risk for Kv11.1 blocking drugs is that multiple ionic channels contribute to cardiac repolarization—the so-called repolarization reserve.[8] Drugs with potency against multiple cardiac ion channels can either reduce or increase the repolarization reserve to modify the level of risk associated with Kv11.1 block[9–11] This concept of multichannel pharmacology has been central to recent efforts by the comprehensive in vitro proarrhythmia assay (CiPA) investigators to develop a more accurate risk stratification workflow based around in silico simulations of the action potential, informed by in vitro screens of multichannel pharmacology.[12–14] These studies proposed a comprehensive measure of potency against 6 cardiac ion channel currents (the fast sodium current (I_{Na}/Nav1.5), late sodium current ($I_{Na,Late}$/toxin-modified Nav1.5), L-type calcium current (I_{CaL}/Cav1.2), Transient outward potassium current (I_{to}/Kv4.3+KChIP2), the inward rectifier potassium current (I_{K1}/Kir2.1), the slow delayed rectifier current (I_{Ks}/KCNQ1 + KCNE1), and the rapid delayed rectifier current (I_{Kr}/Kv11.1) I_{Kr})[13–16] These simulations were then used to derive the "qNet" metric, calculated as the net charge movement across the cardiomyocyte over the duration of the action potential[13] that was able to predict Torsade de Pointes risk more accurately than conventional metrics such as action potential or calcium transient durations.[13] Furthermore, the inclusion in the in silico models of a description of the kinetics of drug binding to hERG, rather than just potency of block, improved categorization of drugs according to their risk classes.[14]

Following this, other studies have explored alternative metrics which also take account of multichannel block. Lancaster and Sobie[17] found that the inclusion of parameters related to calcium transients, in addition to action potential measures, improved risk prediction while Iseppe et al[18] similarly demonstrated the importance of metrics related to calcium handling, particularly in the case of female sex-specific classifiers. Other studies have also explored derivatives of qNet, either alone, or in combination with other measures as predictors of risk.[19,20] However, a potential limitation of metrics such as qNet, is that they cannot be directly measured in vitro—since derivation depends on simulations of each of the individual ionic currents that contribute to the action potential to calculate charge movement. As an alternative, we set out to identify novel metrics for risk prediction that could be directly measured from the voltage waveform. To achieve this, we focussed on the morphology of the repolarization phase of the action potential since (1) simple measures of morphology, such as triangulation[21] have previously been shown to be associated with proarrhythmic risk; (2) the shape of the action potential in response to a drug is a manifestation of the block of multiple ionic channels, so providing a window into multichannel pharmacology (Figure 1A); (3) subtle changes in action potential morphology during repolarization may precede the emergence of ectopic membrane depolarizations, so are mechanistically linked to proarrhythmia (Figure 1B); and (4) the shape of the action potential is driven by the charge movement

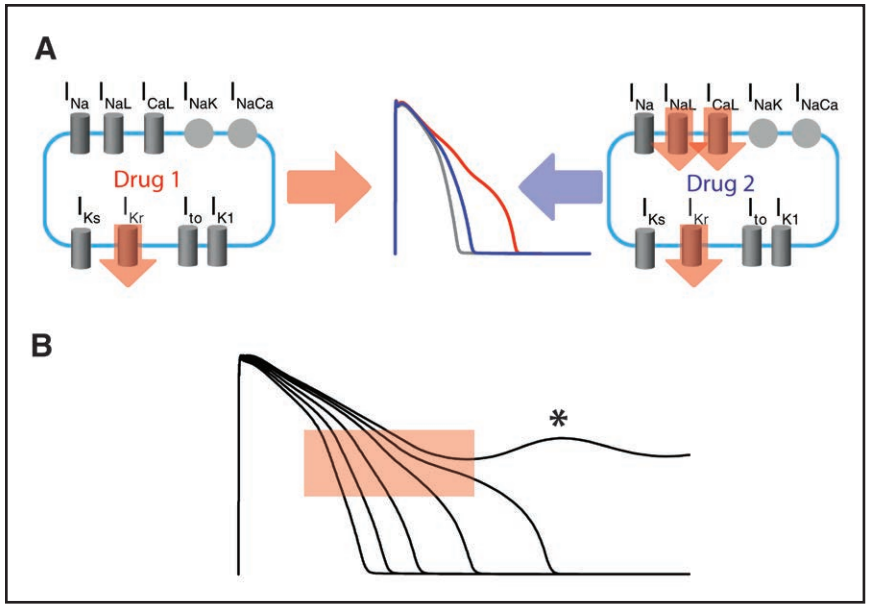

Figure 1. Drug-induced changes to action potential morphology precede emergence of arrhythmia.
A, Schematic showing AP prolongation and morphological changes in response to pure I_{Kr} block (red) or mixed ion channel block (I_{Kr}, I_{CaL}, I_{NaL}; Blue). **B**, Action potentials simulated in response to increasing I_{Kr} block showing changes in waveform morphology (red highlight) preceding emergence of ectopic activity (asterisk).

across the membrane, meaning changes in morphology potentially reflect the same cellular processes measured by qNet that have proved effective in risk allocation. To quantify changes in action potential morphology, we analyzed the radius of curvature of the repolarization phase. Radius of curvature is a method from differential geometry, in which the radius of a circular arc, which best approximates the waveform at each point is measured. A similar approach has previously been applied to electrocardiograms, particularly in relation to identification of T wave notching.[22,23] However, to our knowledge, this is the first application to cellular action potentials.

Using the CiPA panel of 28 drugs, we show that a classifier based on metrics from the radius of curvature signal can more accurately classify proarrhythmic drug risk compared with existing metrics including action potential duration at 90% repolarization (APD_{90}), triangulation and qNet. Furthermore, we demonstrate very high classification accuracy, even in the absence of any description of drug-binding kinetics in action potential simulations. The benefits of this new approach include more accurate risk classification, a reduction in workload associated with the acquisition of complex datasets required to constrain drug-binding kinetics, and the future potential for direct application to action potential waveforms measured in vitro—thereby abolishing the need for screens of potency against multiple ion channels. Together these advances will help accelerate the process of drug development and preclinical safety screening and reduce the costs associated with these assays.

METHODS

In Silico Modelling

Action potentials were simulated in Matlab (Mathworks, MA) using the CiPAORdv1.0[12,16] adaptation of the O'Hara- Rudy model of the ventricular action potential.[24] All data used in the study (simulated action potentials and associated R-signals) are available in Table S1.

Calculation of the Inverse Signed Radius of Curvature signal

To quantify the action potential morphology we used the inverse signed radius of curvature (R) signal[25]:

$$R = \frac{v''}{(1+ v'^2)^{\frac{3}{2}}} \qquad \text{Equation 1}$$

where v' is the first derivative $\frac{dv}{dt}$ and v" is the second derivative $\frac{d^2v}{dt^2}$ of v (where v is membrane potential and t is time).

Features for Classification

For each action potential waveform, 8 timepoints were identified based on the degree of repolarization (AP_{Peak}, APD_{15}, APD_{30}, APD_{45}, APD_{60}, AP_{75}, $APD_{90,}$ and APD_{end}). Based on these timepoints, the repolarization phase was divided into a total of 28 different timespans and for each timespan, the duration of the interval, as well as the area under the R signal (ΣR), were measured from action potentials at both 1 and 0.5 Hz, giving a total of 112 features.

Drug Risk Classification

Risk labels for individual drugs were those assigned by the CiPA clinical translation subgroup,[15] based on published data,[26–28] publicly available data repositories (Credible Meds, FAERS), and FDA labeling. For classification of risk (low, intermediate, and high), multinomial logistic regression was implemented using scikit-learn in Python.[29] Model training was done using data from the twelve drugs in the predetermined training panel, with strict separation from the test panel, before model performance was evaluated on the predetermined test panel. This approach to model assessment is consistent with best practice guidelines[30] and other publications using this dataset[16] and will also facilitate direct comparison of measures of accuracy with other studies using this study design. Classification error for each metric was calculated as the mean (across 16 test drugs)

of the absolute error (difference between predicted and known risk categories), where low risk=1, intermediate risk=2, and high risk=3.

iPSC Culture and Maintenance

Human-induced pluripotent stem cells (iPSC) from healthy patients were obtained from the Stanford University Cardiovascular Institute Biobank. Human-induced pluripotent stem cells were maintained and differentiated as previously described.[31]

Kinetic Imaging Cytometry

Optical action potentials were acquired using voltage-sensitive BeRST dye,[32] a gift from Dr Evan Miller, UC Berkeley, CA using an IC200 kinetic imaging cytometer (Vala Sciences, San Diego, CA). Before the generation of R-signals, optical action potentials were normalized to peak membrane voltage and the repolarization phase fitted using a polynomial function to account for noise.

Ethical Approval and Informed Consent

This project does not include any interaction or intervention with human subjects or include any access to identifiable private information. As a result, it does not require IRB review

RESULTS

Using Curvature to Quantify Changes in Action Potential Morphology

To measure changes in action potential morphology, the inverse signed radius of curvature (R; see methods) was calculated from the repolarization phase of the voltage waveform. At each point, the R signal describes the instantaneous radius length of a theoretical circle which forms a tangent at any given point P along a curve (Figure 2A). A greater rate of change in curvature (tighter curve) will result in a large R signal. Conversely a lower rate of change in curvature (shallower curve) will result in a smaller R signal. Concave-up curves result in a positive R value and concave-down curves result in a negative R value. An example of the R signal derived from a simulated cardiac action potential is shown in Figure 2B where an increasing rate of repolarization results in a negative R signal, and a slowing rate of repolarization or a shift from repolarization to depolarization results in a positive R signal. To quantify the shape of the action potential over discrete time periods of repolarization, the area under the R signal was calculated (∑R). For example, in Figure 2B, the area under the R-signal from APD_{30} to APD_{60} ($\sum R_{30\text{-}60}$) is shaded in red/blue.

Relationship Between I_{Kr} Block and Action Potential Morphology

First, we examined how parameters extracted from the R-signal changed in response to block of I_{Kr} (Figure 3). Action potential waveforms (Figure 3Ai), I_{Kr} current (Figure 3Aii) and associated R-signals (Figure 3Aiii) corresponding to 0%, 50%, and 90% reduction in I_{Kr} conductance are shown in Figure 3A. For simplicity, only 3 consecutive timespans are highlighted (APD_{peak} to APD_{30} [orange], APD_{30} to APD_{60} [cyan] and APD_{60} to APD_{90} [pink]) with the area under the curve (∑R) and the duration of each timespan shown in Aiv and Av, respectively. A summary for the relationship between these measures and I_{Kr} block between 0% and 90% is shown in Figure 3B. Importantly, each parameter has different dependence on the degree of I_{Kr} block. For example, the ∑R for APD_{peak} to APD_{30}, APD_{30} to APD_{60}, and APD_{60} to APD_{90} increase, change sign, and decrease respectively with greater I_{Kr} block.

Relationship Between Changes in Action Potential Morphology and Risk

Next, we investigated whether drug-induced changes in action potential morphology, measured using radius of curvature, reflect torsadogenic risk. Action potential waveforms (Figure 4A), R-signals (Figure 4B), ΣR (Figure 4C), and timespan duration (Figure 4D) for a 3-fold C_{max} dose of typical drugs from the low, intermediate, and high-risk categories of the CiPA training set are shown for the same 3 exemplar timespans illustrated in Figure 3 (action potentials and derived curvature signals for all training and testing drugs are presented in Figures S1 and S2). In this case, the multichannel pharmacology of each drug was incorporated using previously published potencies[10] as well as descriptions of the kinetics of drug binding to hERG.[16,33] Importantly, subtle changes in the shape of the repolarization phase that are difficult to detect and measure on the voltage waveform are clearly reflected in the R signal. For example, the slowing of repolarization that occurs between APD_{30} and APD_{60} in the presence of bepridil results in a clear positive peak in the R signal in this timespan, which is not present for other risk classes. Overall, comparison of the ΣR for each risk category (Figure 4C) shows a distinct pattern associated with each risk category. We therefore examined whether metrics derived from the R signal could be used to build a classifier for assignment of drug risk.

Risk Classification Using Morphology-Based Metrics

To develop a risk classifier based on morphology, we considered a broad range of measures extracted from the R signal at both 1 and 0.5 Hz (see methods, Table S2). Overall, the best performing classifier included descriptions of drug-binding kinetics in the cell model, and combined 3 parameters: (1) the duration of the timespan from APD_{15} to APD_{30} at 1 Hz; (2) ΣR from APD_{15} to APD_{90} at 1 Hz; and (3) the duration of the timespan from APD_{Peak} to APD_{90} at 0.5 Hz (Figure 5A). The distributions of each

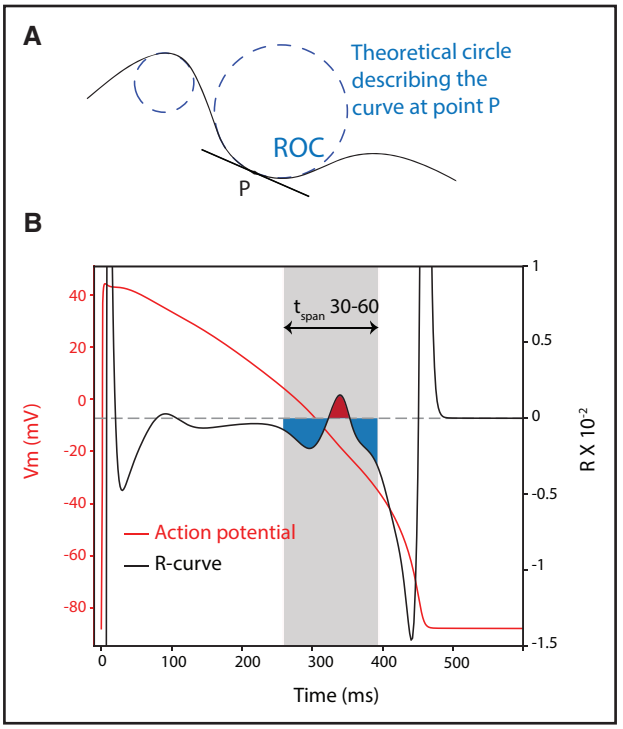

Figure 2. Curvature analysis of cardiac action potential. **A**, Schematic and equation describing curvature signal (R). R is the reciprocal of the radius of a theoretical circle, which touches the curve at a given point P. **B**, R signal (black) for the cardiomyocyte action potential (red). For any timespan (eg, time from 30% to 60% repolarization) an area under the R signal (ΣR) can be calculated (shaded area)

of these parameters for the test (red) and training (blue) drug panels are shown in Figure 5B (Figure S3). If kinetics of drug binding to hERG were not included in the model (ie, hERG block was described as simple reduction in conductance) the optimum combination included just two parameters: ΣR from APD_{15} to APD_{60} at 1 Hz and ΣR from APD_{30} to APD_{90} at 0.5 Hz (Figure S4).

Both morphology-based classifiers (with and without kinetics of drug binding to hERG) performed better than existing metrics including qNet,[13] triangulation,[21] and APD_{90}[34] in 3-way classification of the test set of drugs. The confusion matrices in Figure 6A show that for the morphology+kinetics metric, only a single high-risk drug (disopyramide) was misclassified as intermediate risk (Figure 6Ai). The same drug was also misclassified by Qnet, APD_{90} and triangulation, although in these cases it was classified as low risk (Figure 6Aiii through 6Av). For intermediate risk drugs, both morphology metrics, as well as qNet classified every drug correctly, while APD_{90} and triangulation misclassified 5/7 and 6/7 incorrectly, respectively. Finally, for low-risk drugs, the morphology metrics again classified every drug correctly while qNet, APD_{90} and triangulation misclassified 3/5, 1/5, and 1/5, respectively. Previous studies have also demonstrated the utility of sex-specific classifiers, as well as the requirement for different features in female versus male classifiers.[18]

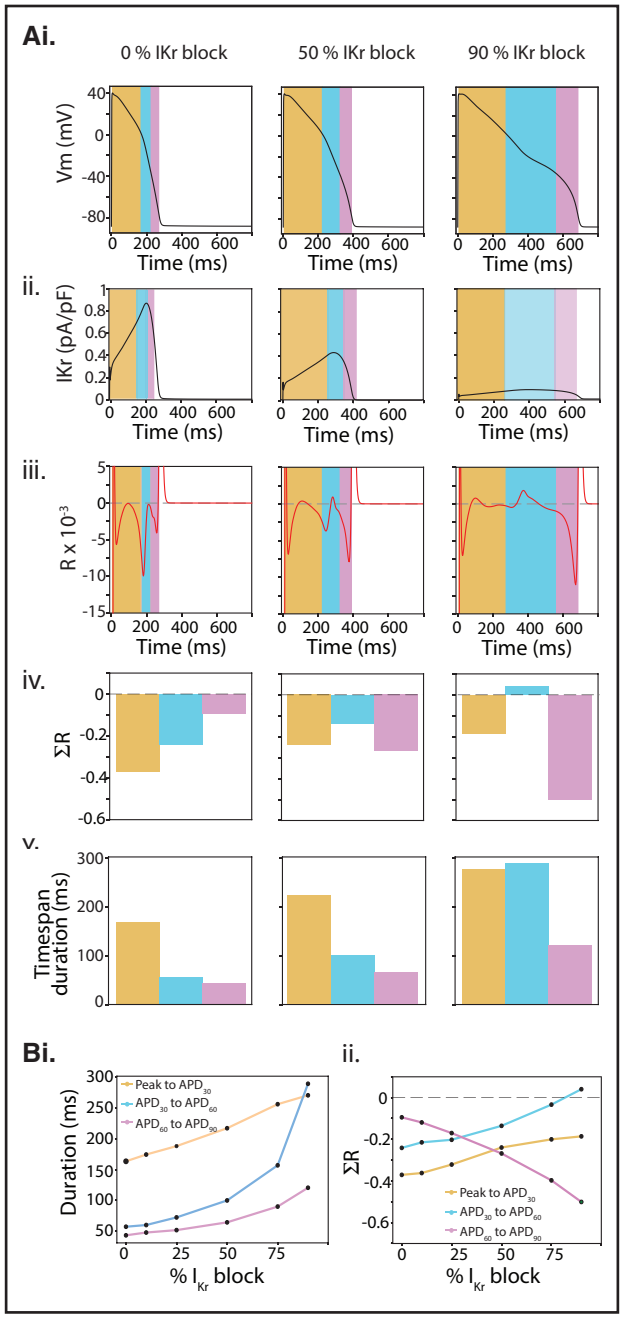

Figure 3. Dependence of curvature on I_{Kr} block. **A**, Action potentials (**i**), I_{Kr} currents (**ii**), R-signals (**iii**), area under R curve (ΣR) (**iv**), and timespan duration (**v**) for 0, 50%, and 90% I_{Kr} block. For illustration, timespans and associated ΣR are shown for action potential peak–30% repolarization (orange), 30% to 60% repolarization (blue), and 60% to 90% repolarization (pink). **B**, Summary plots of timespan duration (**i**) and ΣR (**ii**) as a function of I_{Kr} block.

We therefore also repeated our analysis to identify the best combination of parameters for classification of risk based on simulations of female ventricular cell electrophysiology. In this case, the best classifier had identical accuracy (0.94) to that based on male simulations, albeit with a different combination of features (ΣR from APD_{15}-APD_{90} at 1 Hz, timespan from APD_{peak}-APD_{15} at 1 Hz, and timespan from APD_{15}-APD_{30} at 0.5 Hz; Figure S5).

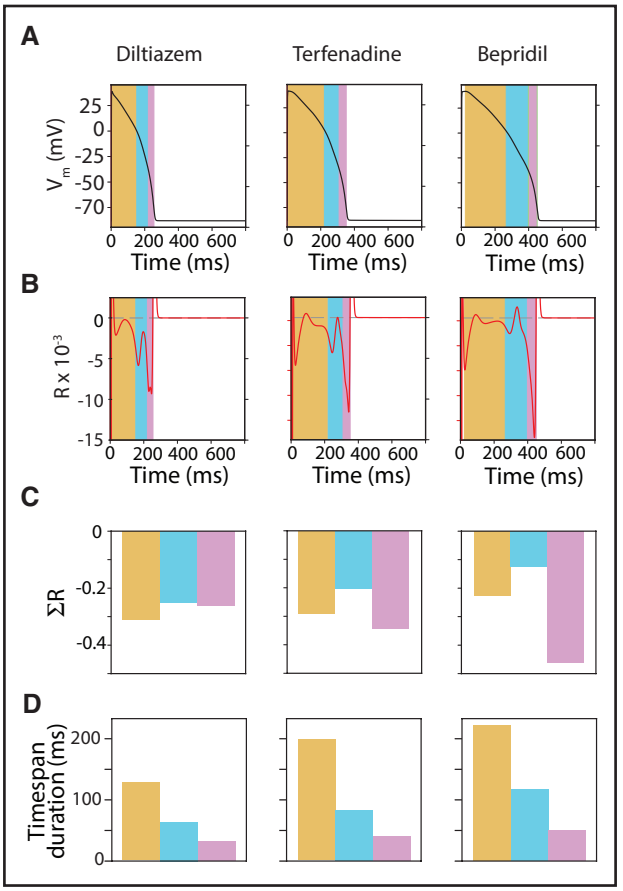

Figure 4. Dependence of curvature on risk class.
A, Action potentials and (**B**) curvature signals for diltiazem (low risk), terfenadine (intermediate risk), and bepridil (high risk) at a concentration of 3-fold C_{max}. **C** and **D**, As an example, ΣR (**C**) and timespan duration (**D**) for action potential peak–30% repolarization (orange), 30% to 60% repolarization (blue), and 60% to 90% repolarization (pink) are shown for each drug risk class.

Of note, only the morphology-based classifiers were able to perfectly separate low risk drugs from other classes (intermediate/high), reflected in an AUC of 1 for the radius of curvature curve (Figure 6B; Table 1), compared with 0.8, 0.818, and 0.836 for qNet, APD_{90}, and triangulation, respectively (Table 1). Overall, classification accuracies were 0.938, 0.875, 0.75, 0.563, and 0.5 for morphology+kinetics, morphology−kinetics, qNet, triangulation, and APD_{90}, respectively (Table 1; Figure 6C). Corresponding error scores were 0.063, 0.125, 0.375, 0.5, and 0.563, respectively, reflecting that in the cases where drugs were misclassified, the degree of misclassification was greater for qNet, triangulation, and APD_{90} than for morphology (Table 1; Figure 6C).

Proof of Concept Application to In Vitro Recorded Action Potentials

To assess whether our method might be applicable to action potentials recorded in vitro, we applied the analysis to action potentials from iPSC-derived cardiomyocytes measured using a voltage-sensitive dye (Berst-1). Typical action potential waveforms recorded from cells exposed to either 500 nmol/L bepridil (a high-risk drug), or 2 μM diltiazem (a low-risk drug), corresponding to a 15-fold C_{max} concentration of each, are shown in Figure 7A. To minimize the effect of signal noise, we fitted the repolarization phase of the action potential with a polynomial function (blue dashed lines, Figure 7A) from which the R-signal was then calculated (red lines, Figure 7A). Data for 3 exemplar parameters (∑R for AP_{peak}-APD_{30}, APD_{30}-APD_{60}, and APD_{60}-APD_{90}) derived from the R-signal of in vitro action potentials (n=19/24 cells for bepridil/diltiazem, respectively) are shown in Figure 7B, along with equivalent parameters derived from in silico action potentials at the same 15-fold C_{max} dose. While there is the expected variability in parameters measured from individual in vitro action potentials, the data show that this approach to measuring morphology of the action potential can be applied to action potentials recorded from cardiomyocytes in vitro.

DISCUSSION

In this study, we describe a new approach to measuring changes in morphology of the cardiac action potential based on the curvature of the voltage waveform. Using metrics derived from the curvature signal, we show that we can assign proarrhythmic risk labels to drugs with potential to prolong repolarization with very high accuracy.

Measurement of Action Potential Morphology Using Curvature Analysis

The concept that changes in morphology of the cardiac action potential might be a window into proarrhythmic risk is well established.[21] Triangulation of the action potential, measured as an increase in the ratio between APD_{30} and APD_{90} in response to drugs that prolongs repolarization, has been associated with increased risk[21] and explored as part of the triangulation, reverse use dependence, instability, dispersion criteria as an approach for detection of drug-induced proarrhythmia.[35,36] However, triangulation is limited as a measure of more complex morphology since the subtleties of shape changes that occur between APD_{30} and APD_{90} are not captured. The corollary of this is that many waveforms, with different shapes, might have the same APD_{30}:APD_{90} ratio meaning much of the information content of the waveforms is lost.

To improve on these established approaches, and more fully quantify shape changes in the action potential waveform, we analyzed the radius of curvature (R) of the repolarization phase. The R-signal essentially measures the concavity of the action potential waveform. More tightly concave phases of the action potential have a greater radius of curvature, with the sign of the curvature

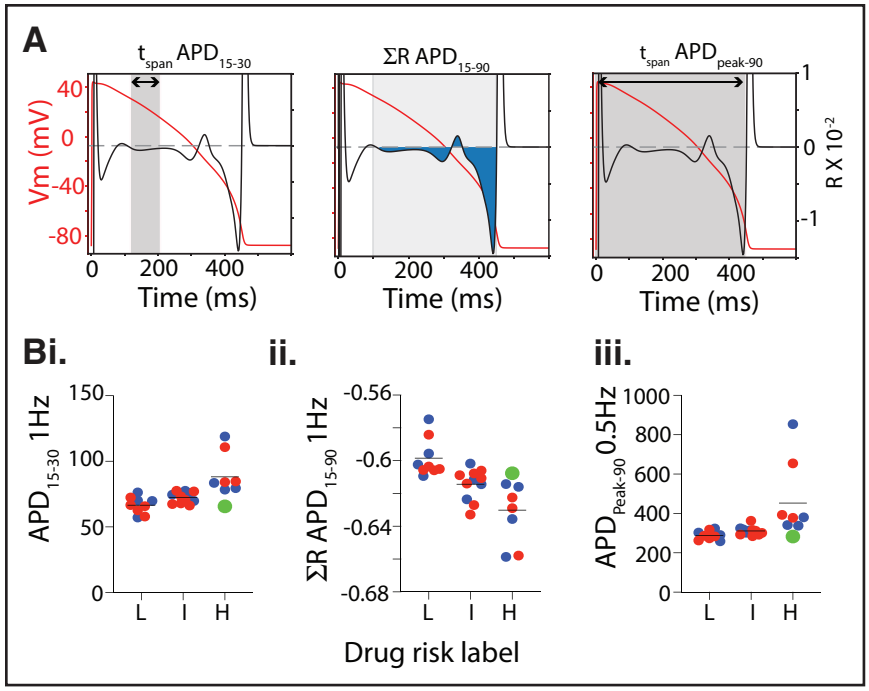

Figure 5. Optimal features selected for classification of test drugs. **A**, Three features that together result in optimal classification of drug risk: timespan from APD_{15} to APD_{30} at 1 Hz (**i**), ΣR from APD_{15} to action potential duration at 90% repolarization (APD_{90}) at 1 Hz (**ii**) and the timespan from AP peak to APD_{90} at 0.5 Hz (**iii**). For each plot, the voltage waveform (red trace, left axis) and receiver operating characteristic curve signal (black trave, right axis) are shown. **B**, Feature distribution for drug risk classes. Datapoints shown in blue and red represent drugs in the CiPA training and test datasets respectively. Datapoint in green represents disopyramide–the only misclassified drug. Average of values for 0.5, 1, 2, and 3-fold Cmax are shown.

signal indicating the direction of concavity. Most significantly, a positive radius of curvature indicates that the action potential is concave up, reflecting that the membrane is being depolarized. We therefore considered that a shift from a negative toward a more positive radius of curvature in the repolarization phase might be an early indicator of the emergence of an early after depolarization (EAD), and so represent a metric that is directly linked to mechanism of arrhythmogenesis and risk.

A Morphology-Based Risk Classifier for Proarrhythmic Drugs

Overall, the most accurate classifier was based on simulations that included the kinetics of drug binding to hERG and combined 3 morphology-related parameters: the duration of the voltage window from 15% to 30% repolarization (APD_{15}:APD_{30}), the area under the R signal (ΣR) from APD_{15} to APD_{90}, and the duration from APD_{peak} to APD_{90} (conventional APD_{90}). This combination classified the test panel with an accuracy of 0.9375 and an error of 0.065. It is interesting to note that despite the unbiased selection of features, this combination is consistent with what we know about cardiac electrophysiology and risk. First, the duration from APD_{15} to APD_{30}, reflects the duration of the plateau, where calcium channels are in the voltage window for reactivation. Second, ΣR from APD_{15} to APD_{90} reflects the overall shape of the repolarization phase and the propensity for ectopic depolarization in response to drugs, and third, APD_{90} has long been a key indicator, albeit imperfect, of proarrhythmia.[37] In relation to APD_{90}, it is perhaps not surprising that this measure of repolarization duration is an important contributor to the optimal metric best metric. Among the 28 CiPA drugs analyzed in this study, most of the unambiguously high-risk drugs prolong APD, and most of the low-risk drugs do not. However, while APD_{90} alone does not perform perfectly in either of these classes (see Figure 6Aiv), perhaps the clearest illustration of what our method adds over and above APD prolongation is in the classification of intermediate drugs. In this case, APD_{90} performs particularly poorly (0.29 sensitivity). By comparison, our metric performs perfectly, with a sensitivity of 1 in this class (Table 1). Overall, the only drug that was labeled incorrectly with this optimum classifier was disopyramide, which was also misclassified in 3 separate studies,[16,20,38] potentially as a result of complex pharmacokinetics in vivo that are not captured in the cell model.[20]

Classification Without Drug-Binding Kinetics

A significant practical limitation to the application of risk assessment pipelines that rely on models of the kinetics of drug binding is the difficulty associated with acquisition of the experimental datasets. For example, the CiPA dynamic protocol[39,40] that has been used to constrain models of drug-binding kinetics for derivation of the qNet metric using the CiPAORdv1.0 model[14,16] is difficult to implement in a robust and reproducible manner, particularly on high-throughput automated patch clamp platforms.[41] We therefore also evaluated the performance of a morphology-based classifier based solely on conduction block (ie, without the inclusion of a description of the kinetics of drug binding to hERG). In this case, the optimum combination of morphology parameters included just 2 measures from the R signal: ΣR from APD_{15} to

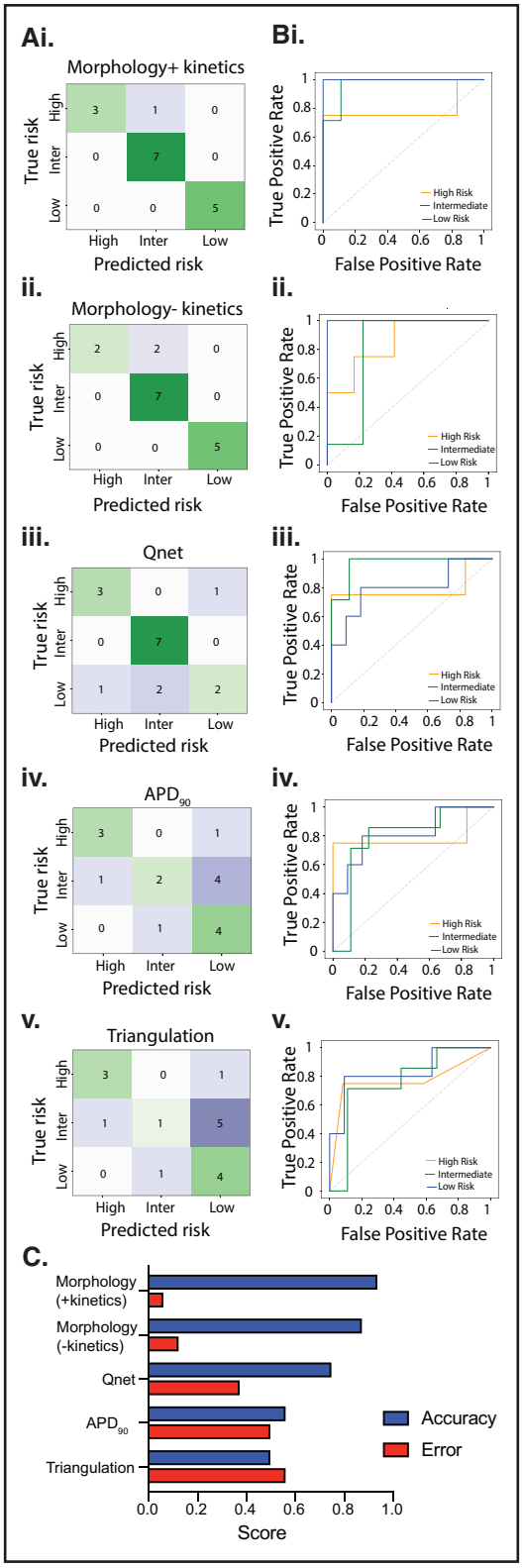

Figure 6. Risk classification.

A, Confusion matrices for 3 drug risk labels (high, intermediate, and low risk) for morphology with and without drug-binding kinetics, Qnet, action potential duration at 90% repolarization (APD_{90}), and triangulation. **B**, Receiver operating characteristic curve curves for low/intermediate/high risk categories for each classifier. **C**, Classifier performance. Accuracy (blue) and error score (red) for classification of the CiPA test set.

APD_{60} at 1 Hz and ΣR from APD_{30} to APD_{90} at 0.5 Hz. These features are quite different from those identified as optimal based on datasets that include drug-binding kinetics. Perhaps most notably, APD_{90} (Timespan of AP_{peak}-APD_{90}), or in fact any measure of timespans, are not in this optimal feature set. This likely reflects that, although these are 2 approaches to describing the same process (drug block of hERG), the observed effects on repolarization for the same concentrations of each drug can be markedly different when kinetics is included versus when it is not (Figure S6), resulting in a different set of optimal features for classification when the model is trained on each of the 2 datasets. Classification accuracy in the absence of kinetics was 0.875. While this corresponds to an additional misclassification compared to when drug-binding kinetics were included (2 versus 1 high-risk drug misclassified at intermediate; Figure 6), it still outperforms all the other metrics tested here (qNet, triangulation, APD_{90}), even when those other metrics were derived from simulations that included drug-binding kinetics. Furthermore, this simpler morphology-based classifier (as well as the more complex version that included kinetics) was able to perfectly separate true low-risk drugs from intermediate/high, which none of the other tested metrics was able to do. Therefore, while the morphology-based classifier performed slightly better than when kinetics was included compared with when without, this is balanced by the fact that the requirement for simpler in vitro datasets potentially makes it a more realistic prospect for preclinical risk prediction.

Link Between Morphology Changes and EADs

One of the key aims of the CiPA initiative was to develop a new metric for risk allocation, mechanistically linked to proarrhythmia,[14,16,30] which would be a more accurate predictor of risk than hERG potency alone. In this regard, several studies have focussed on using the emergence of EADs in simulations of action potential responses to proarrhythmic drugs as potential markers for risk. However, Lopes-Lorente[19] found that a T_{EAD} metric was no better than hERG potency alone in correctly categorizing risk, and similarly, Parikh et al[42,43] found their EAD metric performed relatively poorly. While other studies have demonstrated greater accuracy for EAD related metrics, particularly in the background of population simulations of drug responses[44,45]; in general, this approach has not proven effective. The emergence of an EAD in the ventricular cell model is the final, extreme manifestation of disruption of repolarization. For example, in the O'Hara-Rudy cell model and its derivatives, approximately 90% block of I_{Kr} is required to precipitate an EAD.[24] In this parameter space, model behavior is highly nonlinear, meaning predictions of physiologically relevant drug responses might be challenging. The behavior of the models at these extremes is also relatively unconstrained

Table 1. Classification Scores for Test Panel of 16 Drugs

	Morphology with kinetics				Morphology without kinetics				Q_{net}				APD_{90}				Triangulation			
	H	I	L	Total	H	I	L	Total	H	I	L	Total	H	I	L	Total	H	I	L	Total
Accuracy				0.94				0.88				0.75				0.56				0.5
Error				0.06				0.13				0.38				0.5				0.56
Precision	1	0.88	1		1	0.78	1		0.75	0.78	0.67		0.75	0.67	0.44		0.75	0.5	0.4	
Sensitivity	0.75	1	1		0.5	1	1		0.75	1	0.4		0.75	0.29	0.8		0.75	0.14	0.8	
Specificity	1	0.89	1		1	0.78	1		0.92	0.78	0.91		0.92	0.89	0.55		0.92	0.89	0.45	
F1 score	0.86	0.93	1		0.67	0.88	1		0.75	0.88	0.5		0.75	0.4	0.57		0.75	0.22	0.53	
AUC	0.79	0.97	1		0.85	0.81	1		0.79	0.97	0.8		0.79	0.79	0.82		0.77	0.76	0.84	

APD_{90} indicates action potential duration at 90% repolarization.

since parameterization is typically undertaken at baseline/normal conditions, or in circumstances of moderate disease[46] or mild drug block.[14,16,30] As an alternative, we reasoned that analysis of action potential morphology at a stage before repolarization had become grossly disrupted, might allow detection of subtle changes in the shape of the repolarization phase that precedes the emergence of EADs, so act as an "early warning" marker of risk. Consistent with this, our analysis is based on drug doses between 0.5- and 3-fold C_{max}, a range at which none of the 28 drugs tested cause EADs. This is also broadly consistent with the dose range that has proven most effective in training other recently published classifiers, such as qNet.[16]

Comparison to Existing Metrics

In this study, we compared the performance of morphology-based classifiers to those based on conventional metrics APD_{90} and triangulation, as well as qNet (perhaps the most well-validated of recently published predictors of proarrhythmic risk[13,16]). Our data show that (1) more drugs were correctly classified using morphology; and (2) for those drugs that were misclassified, the degree of misclassification is less (reflected in lower error scores). One of the issues that has been identified as a shortcoming of the standard HERG potency assays, and hence was a motivating factor for CiPA, is the overestimation of risk.[15] In this regard, the sensitivity of our metrics for low-risk drugs was 1, indicating that all low-risk drugs were correctly predicted as such, and not predicted as higher risk. In comparison, the sensitivity of Q_{net} in the low-risk category was 0.4, with 3 of 5 low-risk drugs predicted as either intermediate or high-risk (Table 1). Similarly, of all the metrics tested, our metrics have the highest precision for the high-risk class, indicating that no lower risk drugs were identified as high risk. These scores demonstrate that on this set of test compounds, the issue of overprediction of risk is largely overcome using our metric.

A range of other classification metrics, or combinations thereof, have also been assessed in the literature. Recently, Llopis-Lorente proposed a decision tree approach based on 3 previously published parameters: Tx (the ratio of the drug concentration causing 10% prolongation of APD_{90} to Cmax); TqNet (the ratio of qNET at 10 fold Cmax to control conditions); and Ttriang (a measure of action potential triangulation). Individually, these parameters classified drugs with accuracies of 0.899, 0.908, and 0.917, respectively. When combined this increased to between 0.927 and 0.945, depending on the ion channel targets included in the model. However, these scores are not directly comparable to our study since they relate to binary classification (ie, low versus high risk) of a separate drug panel, and performance was not assessed on a separate test dataset. More comparable is a recent study by Yoo et al who used a combination of 9 parameters derived from the O'Hara cell model (dVm/dt_{max}, $AP_{resting}$, APD90, APD_{50}, $Ca_{resting}$, CaD_{90}, CaD_{50}, qNet, and qInward) as inputs for a neural network classifier that was trained on the 12 drug CiPA test panel and tested on the 16 drug test panel. Using that approach, 4 drugs were incorrectly classified (disopyramide, azimalide, loratadine and tamoxifen), corresponding to an accuracy of 0.75 and an error of 0.25. Overall then, our morphology-based classifier, even without inclusion of drug-binding kinetics, performs better than other directly comparable published methods applied to the CiPA drug panels.

Potential for Direct Measurement From Voltage Waveforms

A general issue with in silico based classifiers, such as that described here and those published as part of CiPA[16] and in other studies,[19,20] is the significant cost, time and technical burden of in vitro data collection required to inform the models—that is, the measures of potency and binding kinetics against multiple cardiac ion channels. The measurement of kinetics, in particular, has proven difficult to implement,[47] particularly on high-throughput patch clamp platforms. However, while the method described here is based on simulated action potentials, a potential future implementation is that the metric could be derived directly from in vitro action potential waveforms. This has 2 major advantages. First, there is no requirement for screening for potency or kinetics in

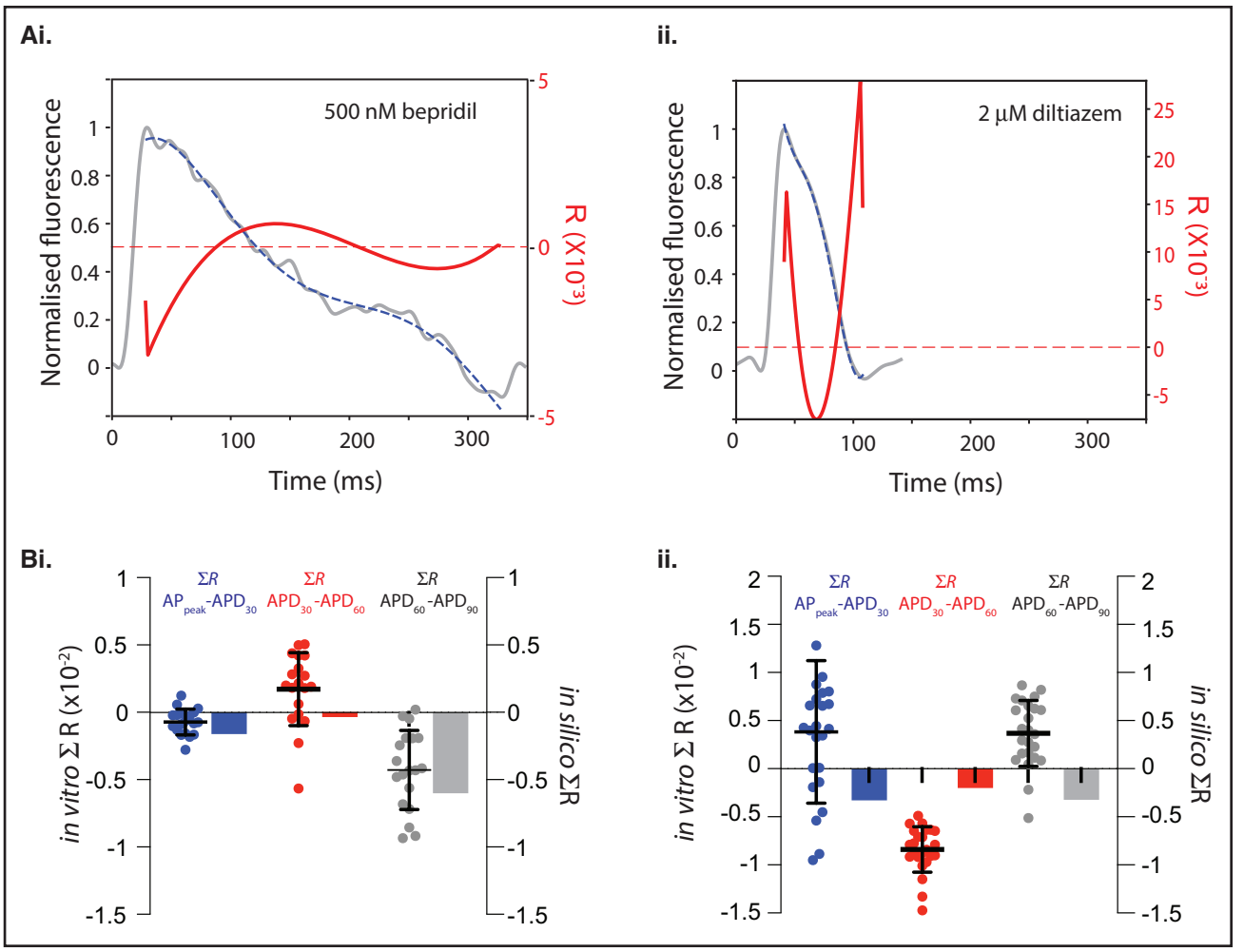

Figure 7. Proof of concept application of curvature analysis to in vitro action potentials.
A, Typical action potential waveforms (gray) recorded from iPSC cardiomyocytes in response to a 15-fold C_{max} concentration of bepridil (**i**) and diltiazem (**ii**). Polynomial fits to repolarization phase (blue dashed) and R-signals (red) are shown in each case. **B**, Comparison of exemplar features extracted from the R-signal of in vitro action potentials with their in silico equivalents. N=19/24 cells for bepridil/diltiazem, respectively.

multiple assays to generate input data. Rather, a single assay measuring effects on repolarization in cardiomyocytes could be undertaken. This is particularly attractive since these in vitro cardiomyocyte assays, using either acutely isolated or iPSC-derived cardiomyocytes are already routinely used to measure repolarization effects (APD_{90}) as part of preclinical assays under S7B and in the case of IPSC-derived cardiomyocytes have recently been evaluated as part of the CiPA paradigm.[48] Second, multiple outputs of the in silico model—such as different ion channel currents, calcium transient characteristics and voltage parameters—do not need to be calculated as part of the metric as is the case with many previously reported classifiers.[20,43] A direct measurement of curvature would therefore yield significant time and cost savings. To assess the feasibility of such an approach, we therefore undertook a proof of principle application of curvature analysis to action potentials recorded in vitro from iPSC cardiomyocytes. Overall, there was good agreement in the trends and amplitudes of ΣR measures for high- and low-risk drugs between in vitro and in silico analysis. This was particularly true for bepridil, where there was a strikingly good correlation between the 2 techniques (Figure 7Bi). For diltiazem, there was more divergence between in vitro and in silico measures, with ΣR APD_{30}-APD_{60} in particular being much more negative in the in vitro case, reflecting faster repolarization in the iPSC cardiomyocytes relative to the in silico model. One possible explanation for this would be a difference in the expression and hence relative contribution to repolarization, of calcium channels between the 2 systems—manifesting as a different response to calcium channel block by diltiazem. Overall then, this proof of concept data demonstrates, that with consideration of compensating for signal noise, the analysis we have developed here in silico can be successfully applied to action potentials recorded from cardiomyocytes in vitro. However, to realize this, it will undoubtedly be necessary to train classifiers based on morphology metrics measured from full in vitro drug response datasets as part of future studies.

Limitations

Any approach to classification based on simulated action potentials is ultimately dependent on the input data—the measured potency against cardiac ion channels. In this study, the range of channels was limited to those measured for the CIPA drug panels: I_{Na}, $I_{Na,Late}$, $I_{Ca,L}$, I_{to}, I_{K1}, I_{Ks}, and I_{Kr}. Other studies have previously shown that other membrane conductances, particularly the sodium-potassium pump (I_{NaK}) and the Sodium Calcium exchanger (I_{NaCa}) are important in the genesis of arrhythmias.[17,49] To our knowledge, there are no published drug datasets reporting activity against these targets (in addition to the ion channel studied here) so it remains to be seen whether the incorporation of additional potencies might alter classifier performance. A second limitation of the input data is the uncertainty in these measures of potency—that is, to what extent can we be confident that the measured potency is a true reflection of activity against a particular ion channel target. The importance of such data variability in proarrhythmic risk assessment was recently demonstrated by Chang et al.[12] It is also well documented that measured potencies can vary dramatically between studies[15] depending on factors such as voltage protocol, or assay platform used.[47,50] This is therefore an important consideration in application of any approach to proarrhythmic risk prediction. Finally, the drug panel used in this study is relatively small (28 drugs). While ideally a larger set of training and testing drugs might be used, we chose to use the CiPA panel since it has the most comprehensive measures of potency across cardiac ion channel targets, is thoroughly characterized in terms of discrete risk labels, and has predetermined allocation to training and testing drugs.

Conclusions

In this study, we describe the application of curvature analysis as a novel approach to measuring morphology of the cardiac action potential, particularly in relation to shape changes in the repolarization phase that occur as precursors to early after depolarizations. We show that metrics derived from the curvature signal can categorise risk of proarrhythmic drugs from the CiPA panel with very high accuracy, outperforming existing metrics. Furthermore, curvature analysis could be applied directly to action potentials measured in vitro, significantly reducing the data collection burden of measuring potency against panels of cardiac ion channels. Overall, our data suggest that measurement of morphological changes in the action potential waveform has significant potential as a new approach to the assessment of proarrhythmic risk in preclinical drug development.

ARTICLE INFORMATION

Received September 19, 2022; accepted June 8, 2023.

Affiliations

Victor Chang Cardiac Research Institute, Sydney, Australia (B.N., M.M.M., M.D.P., R.N.S., J.I.V., A.P.H.). School of Clinical Medicine, Faculty of Medicine and Health, UNSW Sydney, Australia (W.L.,B.N., M.M.M., R.N.S., J.I.V., A.P.H.). Department of Pharmacology, School of Medical Sciences, UNSW Sydney, Sydney, Australia (M.D.P.).

Acknowledgments

We acknowledge the Victor Chang Cardiac Research Institute Cardiovascular Innovation Center, supported by NSW Health.

Sources of Funding

This study was supported by Australian National Health and Medical Research Council grant APP1182623 and a NSW Health cardiovascular capacity building grant to Dr Hill.

Disclosures

None.

Supplemental Material

Supplemental Methods
Tables S1 and S2
Figures S1–S6
References [51,52]

REFERENCES

1. Roden DM. Drug-induced prolongation of the QT interval. *N Engl J Med*. 2004;350:1013–1022. doi: 10.1056/NEJMra032426
2. Gintant G, Sager PT, Stockbridge N. Evolution of strategies to improve preclinical cardiac safety testing. *Nat Rev Drug Discov*. 2016;15:457–471. doi: 10.1038/nrd.2015.34
3. Perrin MJ, Subbiah RN, Vandenberg JI, Hill AP. Human ether-a-go-go related gene (hERG) K+ channels: function and dysfunction. *Prog Biophys Mol Biol*. 2008;98:137–148. doi: 10.1016/j.pbiomolbio.2008.10.006
4. Food and Drug Administration, HHS. International Conference on Harmonisation; guidance on E14 Clinical Evaluation of QT/QTc Interval Prolongation and Proarrhythmic Potential for Non-Antiarrhythmic Drugs. *Notice Fed Regist*. 2005 Oct 20;70(202):61134–5. PMID: 16237860.
5. Food and Drug Administration, HHS. International Conference on Harmonisation; guidance on S7B Nonclinical Evaluation of the Potential for Delayed Ventricular Repolarization (QT Interval Prolongation) by Human Pharmaceuticals. *Notice Fed Regist*. 2005 Oct 20;70(202):61133–4. PMID: 16237859.
6. De Ponti F, Poluzzi E, Montanaro N. Organising evidence on QT prolongation and occurrence of Torsades de Pointes with non-antiarrhythmic drugs: a call for consensus. *Eur J Clin Pharmacol*. 2001;57:185–209. doi: 10.1007/s002280100290
7. Sager PT, Gintant G, Turner JR, Pettit S, Stockbridge N. Rechanneling the cardiac proarrhythmia safety paradigm: a meeting report from the Cardiac Safety Research Consortium. *Am Heart J*. 2014;167:292–300. doi: 10.1016/j.ahj.2013.11.004
8. Roden DM. Mechanisms and management of proarrhythmia. *Am J Cardiol*. 1998;82:49I–57I. doi: 10.1016/s0002-9149(98)00472-x
9. Bril A, Gout B, Bonhomme M, Landais L, Faivre JF, Linee P, Poyser RH, Ruffolo RR Jr. Combined potassium and calcium channel blocking activities as a basis for antiarrhythmic efficacy with low proarrhythmic risk: experimental profile of BRL-32872. *J Pharmacol Exp Ther*. 1996;276:637–646.
10. Crumb WJ Jr, Vicente J, Johannesen L, Strauss DG. An evaluation of 30 clinical drugs against the comprehensive in vitro proarrhythmia assay (CiPA) proposed ion channel panel. *J Pharmacol Toxicol Methods*. 2016;81:251–262. doi: 10.1016/j.vascn.2016.03.009
11. Martin RL, Su Z, Limberis JT, Palmatier JD, Cowart MD, Cox BF, Gintant GA. In vitro preclinical cardiac assessment of tolterodine and terodiline: multiple factors predict the clinical experience. *J Cardiovasc Pharmacol*. 2006;48:199–206. doi: 10.1097/01.fjc.0000246853.15926.d4
12. Chang KC, Dutta S, Mirams GR, Beattie KA, Sheng J, Tran PN, Wu M, Wu WW, Colatsky T, Strauss DG, et al. Uncertainty quantification reveals the importance of data variability and experimental design considerations for in silico proarrhythmia risk assessment. *Front Physiol*. 2017;8:917. doi: 10.3389/fphys.2017.00917
13. Dutta S, Chang KC, Beattie KA, Sheng J, Tran PN, Wu WW, Wu M, Strauss DG, Colatsky T, Li Z. Optimization of an in silico cardiac cell model for proarrhythmia risk assessment. *Front Physiol*. 2017;8:616. doi: 10.3389/fphys.2017.00616

14. Li Z, Dutta S, Sheng J, Tran PN, Wu W, Chang K, Mdluli T, Strauss DG, Colatsky T. Improving the in silico assessment of proarrhythmia risk by combining hERG (Human Ether-a-go-go-Related Gene) channel-drug binding kinetics and multichannel pharmacology. *Circ Arrhythm Electrophysiol*. 2017;10:e004628. doi: 10.1161/CIRCEP.116.004628
15. Fermini B, Hancox JC, Abi-Gerges N, Bridgland-Taylor M, Chaudhary KW, Colatsky T, Correll K, Crumb W, Damiano B, Erdemli G, et al. A new perspective in the field of cardiac safety testing through the comprehensive in vitro proarrhythmia assay paradigm. *J Biomol Screen*. 2016;21:1–11. doi: 10.1177/1087057115594589
16. Li Z, Ridder BJ, Han X, Wu WW, Sheng J, Tran PN, Wu M, Randolph A, Johnstone RH, Mirams GR, et al. Assessment of an in silico mechanistic model for proarrhythmia risk prediction under the CiPA initiative. *Clin Pharmacol Ther*. 2019;105:466–475. doi: 10.1002/cpt.1184
17. Lancaster MC, Sobie EA. Improved prediction of drug-induced torsades de pointes through simulations of dynamics and machine learning algorithms. *Clin Pharmacol Ther*. 2016;100:371–379. doi: 10.1002/cpt.367
18. Fogli Iseppe A, Ni H, Zhu S, Zhang X, Coppini R, Yang PC, Srivatsa U, Clancy CE, Edwards AG, Morotti S, et al. Sex-specific classification of drug-induced torsade de pointes susceptibility using cardiac simulations and machine learning. *Clin Pharmacol Ther*. 2021;110:380–391. doi: 10.1002/cpt.2240
19. Llopis-Lorente J, Gomis-Tena J, Cano J, Romero L, Saiz J, Trenor B. In silico classifiers for the assessment of drug proarrhythmicity. *J Chem Inf Model*. 2020;60:5172–5187. doi: 10.1021/acs.jcim.0c00201
20. Yoo Y, Marcellinus A, Jeong DU, Kim KS, Lim KM. Assessment of drug proarrhythmicity using artificial neural networks with in silico deterministic model outputs. *Front Physiol*. 2021;12:761691. doi: 10.3389/fphys.2021.761691
21. Hondeghem LM, Carlsson L, Duker G. Instability and triangulation of the action potential predict serious proarrhythmia, but action potential duration prolongation is antiarrhythmic. *Circulation*. 2001a;103:2004–2013. doi: 10.1161/01.cir.103.15.2004
22. Porta-Sanchez A, Spillane DR, Harris L, Xue J, Dorsey P, Care M, Chauhan V, Gollob MH, Spears DA. T-wave morphology analysis in congenital long QT syndrome discriminates patients from healthy individuals. *JACC Clin Electrophysiol*. 2017;3:374–381. doi: 10.1016/j.jacep.2016.10.013
23. Vicente J, Johannesen L, Mason JW, Crumb WJ, Pueyo E, Stockbridge N, Strauss DG. Comprehensive T wave morphology assessment in a randomized clinical study of dofetilide, quinidine, ranolazine, and verapamil. *J Am Heart Assoc*. 2015;4:e001615. doi: 10.1161/JAHA.114.001615
24. O'Hara T, Virág L, Varró A, Rudy Y. Simulation of the undiseased human cardiac ventricular action potential: model formulation and experimental validation. *PLoS Comp Biol*. 2011;7:e1002061. doi: 10.1371/journal.pcbi.1002061
25. Andersen MP, Xue JQ, Graff C, Hardahl TB, Toft E, Kanters JK, Christiansen M, Jensen HK, Struijk JJ. A robust method for quantification of IKr-related T-wave morphology abnormalities. *Comput Cardiol*. 2007;34:341-344. doi: 10.1109/CIC.2007.4745491
26. Kramer J, Obejero-Paz CA, Myatt G, Kuryshev YA, Bruening-Wright A, Verducci JS, Brown AM. MICE models: superior to the HERG model in predicting Torsade de Pointes. *Sci Rep*. 2013;3:2100. doi: 10.1038/srep02100
27. Mirams GR, Cui Y, Sher A, Fink M, Cooper J, Heath BM, McMahon NC, Gavaghan DJ, Noble D. Simulation of multiple ion channel block provides improved early prediction of compounds' clinical torsadogenic risk. *Cardiovasc Res*. 2011;91:53–61. doi: 10.1093/cvr/cvr044
28. Redfern WS, Carlsson L, Davis AS, Lynch WG, MacKenzie I, Palethorpe S, Siegl PK, Strang I, Sullivan AT, Wallis R, et al. Relationships between preclinical cardiac electrophysiology, clinical QT interval prolongation and torsade de pointes for a broad range of drugs: evidence for a provisional safety margin in drug development. *Cardiovasc Res*. 2003;58:32–45. doi: 10.1016/s0008-6363(02)00846-5
29. Pedregosa F, Varoquanx G, Gramfort A, Michel V, Thirion B, Grisel O, Blondel M, Prettenhofer P, Weiss R, Dubourg V, et al. Scikit-learn: machine learning in python. *J Mach Learn Res*. 2011;12:2825–2830.
30. Li Z, Mirams GR, Yoshinaga T, Ridder BJ, Han X, Chen JE, Stockbridge NL, Wisialowski TA, Damiano B, Severi S, et al. General principles for the validation of proarrhythmia risk prediction models: an extension of the CiPA in silico strategy. *Clin Pharmacol Ther*. 2020;107:102–111. doi: 10.1002/cpt.1647
31. Perry MD, Ng CA, Mangala MM, Ng TYM, Hines AD, Liang W, Xu MJO, Hill AP, Vandenberg JI. Pharmacological activation of IKr in models of long QT Type 2 risks overcorrection of repolarization. *Cardiovasc Res*. 2020;116:1434–1445. doi: 10.1093/cvr/cvz247
32. Huang YL, Walker AS, Miller EW. A photostable silicon rhodamine platform for optical voltage sensing. *J Am Chem Soc*. 2015;137:10767–10776. doi: 10.1021/jacs.5b06644
33. Li Z, Dutta S, Sheng J, Tran PN, Wu W, Colatsky T. A temperature-dependent in silico model of the human ether-a-go-go-related (hERG) gene channel. *J Pharmacol Toxicol Methods*. 2016;81:233–239. doi: 10.1016/j.vascn.2016.05.005
34. Osadchii OE. Dofetilide promotes repolarization abnormalities in perfused Guinea-pig heart. *Cardiovasc Drugs Ther*. 2012;26:489–500. doi: 10.1007/s10557-012-6405-1
35. Hondeghem LM. TRIad: foundation for proarrhythmia (triangulation, reverse use dependence and instability). *Novartis Found Symp*. 2005;266:235–44; discussion 244. doi: 10.1002/047002142X.ch18
36. Shah RR. Drug-induced QT interval prolongation--regulatory guidance and perspectives on hERG channel studies. *Novartis Found Symp*. 2005;266:251–80; discussion 280. doi: 10.1002/047002142X.ch19
37. Kato R, Ikeda N, Yabek SM, Kannan R, Singh BN. Electrophysiologic effects of the levo- and dextrorotatory isomers of sotalol in isolated cardiac muscle and their in vivo pharmacokinetics. *J Am Coll Cardiol*. 1986;7:116–125. doi: 10.1016/s0735-1097(86)80268-6
38. Han S, Han S, Kim KS, Lee HA, Yim DS. Usefulness of Bnet, a simple linear metric in discerning torsades de pointes risks in 28 CiPA drugs. *Front Pharmacol*. 2019;10:1419. doi: 10.3389/fphar.2019.01419
39. Milnes JT, Witchel HJ, Leaney JL, Leishman DJ, Hancox JC. Investigating dynamic protocol-dependence of hERG potassium channel inhibition at 37 degrees C: cisapride versus dofetilide. *J Pharmacol Toxicol Methods*. 2010;61:178–191. doi: 10.1016/j.vascn.2010.02.007
40. Windley MJ, Abi-Gerges N, Fermini B, Hancox JC, Vandenberg JI, Hill AP. Measuring kinetics and potency of hERG block for CiPA. *J Pharmacol Toxicol Methods*. 2017;87:99–107. doi: 10.1016/j.vascn.2017.02.017
41. Windley MJ, Farr J, TeBay C, Vandenberg JI, Hill AP. High throuput measurement of hERG drug block kinetics using the CiPA dynamic protocol. *J Pharmacol Toxicol Methods*. 2022;117:107192. doi: 10.1016/j.vascn.2022.107192
42. Parikh J, Di Achille P, Kozloski J, Gurev V. Global sensitivity analysis of ventricular myocyte model-derived metrics for proarrhythmic risk assessment. *Front Pharmacol*. 2019;10:1054. doi: 10.3389/fphar.2019.01054
43. Parikh J, Gurev V, Rice JJ. Novel two-step classifier for torsades de pointes risk stratification from direct features. *Front Pharmacol*. 2017;8:816. doi: 10.3389/fphar.2017.00816
44. Britton OJ, Bueno-Orovio A, Virag L, Varro A, Rodriguez B. The electrogenic Na(+)/K(+) pump is a key determinant of repolarization abnormality susceptibility in human ventricular cardiomyocytes: a population-based simulation study. *Front Physiol*. 2017;8:278. doi: 10.3389/fphys.2017.00278
45. Muszkiewicz A, Britton OJ, Gemmell P, Passini E, Sanchez C, Zhou X, Carusi A, Quinn TA, Burrage K, Bueno-Orovio A, et al. Variability in cardiac electrophysiology: using experimentally-calibrated populations of models to move beyond the single virtual physiological human paradigm. *Prog Biophys Mol Biol*. 2016;120:115–127. doi: 10.1016/j.pbiomolbio.2015.12.002
46. Mann SA, Imtiaz M, Winbo A, Rydberg A, Perry MD, Couderc JP, Polonsky B, McNitt S, Zareba W, Hill AP, et al. Convergence of models of human ventricular myocyte electrophysiology after global optimization to recapitulate clinical long QT phenotypes. *J Mol Cell Cardiol*. 2016;100:25–34. doi: 10.1016/j.yjmcc.2016.09.011
47. Kramer J, Himmel HM, Lindqvist A, Stoelzle-Feix S, Chaudhary KW, Li D, Bohme GA, Bridgland-Taylor M, Hebeisen S, Fan J, et al. Cross-site and cross-platform variability of automated patch clamp assessments of drug effects on human cardiac currents in recombinant cells. *Sci Rep*. 2020;10:5627. doi: 10.1038/s41598-020-62344-w
48. Pfeiffer-Kaushik ER, Smith GL, Cai B, Dempsey GT, Hortigon-Vinagre MP, Zamora V, Feng S, Ingermanson R, Zhu R, Hariharan V, et al. Electrophysiological characterization of drug response in hSC-derived cardiomyocytes using voltage-sensitive optical platforms. *J Pharmacol Toxicol Methods*. 2019;99:106612. doi: 10.1016/j.vascn.2019.106612
49. Nagy N, Kormos A, Kohajda Z, Szebeni A, Szepesi J, Pollesello P, Levijoki J, Acsai K, Virag L, Nanasi PP, et al. Selective Na(+)/Ca(2+) exchanger inhibition prevents Ca(2+) overload-induced triggered arrhythmias. *Br J Pharmacol*. 2014;171:5665–5681. doi: 10.1111/bph.12867
50. Lee W, Windley MJ, Perry MD, Vandenberg JI, Hill AP. Protocol-dependent differences in IC50 values measured in human ether-A-go-go-related gene assays occur in a predictable way and can be used to quantify state preference of drug binding. *Mol Pharmacol*. 2019;95:537–550. doi: 10.1124/mol.118.115220
51. Yang PC, Clancy CE. In silico prediction of sex-based differences in human susceptibility to cardiac ventricular tachyarrhythmias. *Front Physiol*. 2012;3:360. doi: 10.3389/fphys.2012.00360
52. TeBay C, McArthur JR, Mangala M, Kerr N, Heitmann S, Perry MD, Windley MJ, Vandenberg JI, Hill AP. Pathophysiological metabolic changes associated with disease modify the proarrhythmic risk profile of drugs with potential to prolong repolarisation. *Br J Pharmacol*. 2022;179:2631–2646. doi: 10.1111/bph.15757